Wenchun Jiang*, Shaohua Li, Yun Luo and Shugen Xu

Creep Damage Analysis of a Lattice Truss Panel Structure

DOI 10.1515/htmp-2015-0189
Received September 2, 2015; accepted December 19, 2015

Abstract: The creep failure for a lattice truss sandwich panel structure has been predicted by finite element method (FEM). The creep damage is calculated by three kinds of stresses: as-brazed residual stress, operating thermal stress and mechanical load. The creep damage at tensile and compressive loads have been calculated and compared. The creep rate calculated by FEM, Gibson–Ashby and Hodge–Dunand models have been compared. The results show that the creep failure is located at the fillet at both tensile and creep loads. The damage rate at the fillet at tensile load is 50 times as much as that at compressive load. The lattice truss panel structure has a better creep resistance to compressive load than tensile load, because the creep and stress triaxiality at the fillet has been decreased at compressive load. The maximum creep strain at the fillet and the equivalent creep strain of the panel structure increase with the increase of applied load. Compared with Gibson–Ashby model and Hodge–Dunand models, the modified Gibson–Ashby model has a good prediction result compared with FEM. However, a more accurate model considering the size effect of the structure still needs to be developed.

Keywords: lattice truss structure, creep damage, finite element

PACS® (2010). 81.40. Lm Creep

Introduction

Lightweight lattice truss sandwich panel structure has a good application trend at high temperatures because they have high load bearing, high strength and good creep resistance, etc. [1–3]. Another outstanding advantage is that it has a high surface area density and can be used to fabricate heat exchanger with high efficiency for active cooling [4, 5]. In the modern steam turbine, it is essential to improve thermal efficiency by increasing the steam temperature and pressure. At high temperature, creep strength should be ensured but the present plant materials have reached their operation limit. Therefore, designing the lattice truss sandwich panel structure as the steam turbine casing can reduce the material temperature to tolerable conditions [6]. Another, the lattice truss sandwich panel structure has a potential for recuperator and intermediate heat exchanger for high temperature gas-cooled reactor (HTGR) [7–9]. For modern steam turbine and HTGR, the operating temperature is very high and the structures are primarily subjected to creep deformation, and the creep failure will be the main failure mode at high temperature [10, 11]. Therefore, it is very important to study the creep strength of lattice truss sandwich panel structure.

The creep strength of compact heat exchanger has attracted a lot of attention in recent years. Nobutada Ohno et al. [12–15] studied the elastic-viscoplastic behavior of plate-fin structure by a homogenized method. F. Kawashima et al. [16] studied the high temperature strength and inelastic behavior of plate-fin structure by equivalent-homogeneous-solid concept. Zhou and Tu [17] studied the time-dependent deformation and stresses of the plate-fin structure by assuming the fins as elastic springs. We [18, 19] studied the effect of brazed residual stress on creep for plate fin structure by finite element analysis. Scott and Dunand [20] studied the creep deformation in cellular metals by FEM for 3D unit cell. EI-Emgd et al. [8, 21] studied the creep behavior of P92 wire mesh sandwich structure by FEM, and they proposed a model to predict the points of time when spontaneous weld spot failure occurs. In this paper, we performed creep damage analysis to lattice truss sandwich panel structure by FEM, and the results were also compared to the analytical models. The effect of applied load on the equivalent macro creep strain and the local damage was also analyzed for tensile and compressive loads.

Finite element model

Geometrical model and meshing

Figure 1 shows the schematic of the X-type lattice truss sandwich panel structure. The core is a lattice truss

*Corresponding author: Wenchun Jiang, State Key Laboratory of Heavy Oil Processing, College of Chemical Engineering, China University of Petroleum (East China), Qingdao 266580, PR China, E-mail: jiangwenchun@126.com
Shaohua Li, Yun Luo, Shugen Xu, State Key Laboratory of Heavy Oil Processing, College of Chemical Engineering, China University of Petroleum (East China), Qingdao 266580, PR China

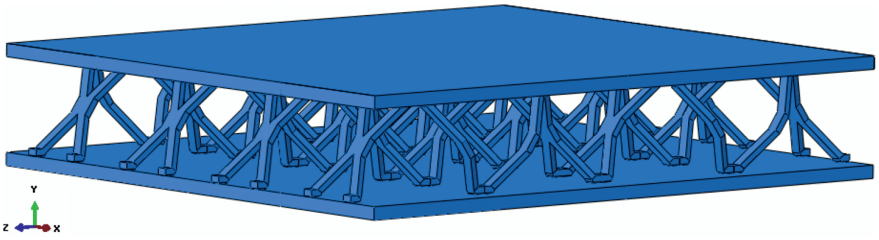

Figure 1: Schematic of the X-type lattice truss sandwich panel structure.

structure formed by punching a diamond pattern sheet. This periodic diamond pattern sheet is fabricated by the slitting, expanding and flattening method [22, 23]. Punching continuously at the middle of the edge of the diamond sheet can form the X-type lattice structure. Then the panel structure is fabricated by brazing the core to the face sheet by a filler metal.

As shown in Figure 1, the lattice truss panel structure is very complex. It contains a lot of trusses, brazing joints and geometrical discontinuities. The joint thickness is at micrometer scale, while the truss is at millimeter scale and the macro length of the structure is even likely to be meter scale, which belongs to a typical multiscale structure. If we build a finite element model with full dimension, it will generate a large number of nodes and elements and cost a long time to calculate. But the characteristic is that it belongs to a periodic structure, and we can build a simple model of unit cell, e. g. by considering the stress concentration at nodes and by using periodic boundary conditions.

Figure 2 shows the finite element model of a unit cell. Where t, l and w are the thickness, length and width of the truss respectively; b is the node size; ω and β are the inclination angle. A three-dimensional FE model is built by ABAQUS code and its meshing is shown in Figure 3. The meshing around the brazing joint is fine and then becomes coarse far away. The effect of number of elements on calculation results has been examined. In total, 25,940 nodes and 19,668 elements are meshed. The element type for creep and stress calculation is C3D8.

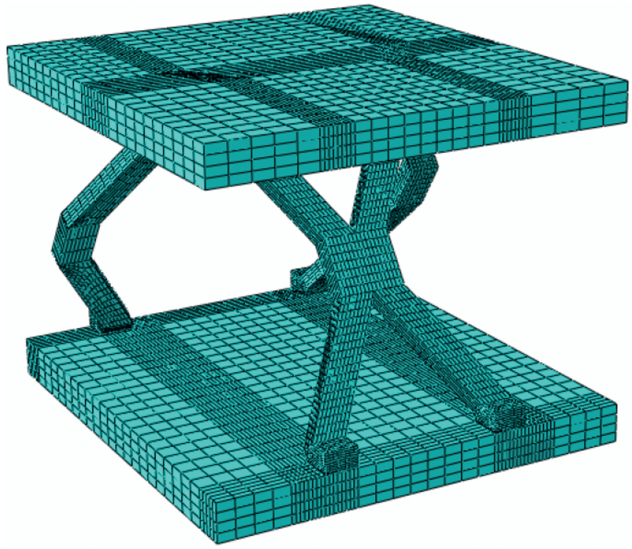

Figure 3: Finite element meshing.

Creep damage model

The creep damage is analyzed by using creep law material parameters determined from bulk material. The creep constitutive equation is Norton equation [24]:

$$\dot{\varepsilon}_c = \dot{B}\sigma^n \tag{1}$$

where the ε_c is the strain rate (s^{-1}); σ is stress (MPa), B and n are material constants.

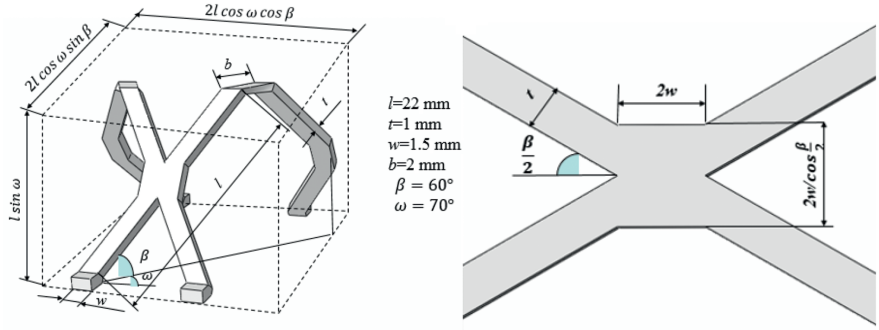

Figure 2: Finite element model of a unit cell.

The creep damage is calculated by the ductility exhaustion approach [25, 26]:

$$D = \frac{\varepsilon_e}{\varepsilon_f^*} \tag{2}$$

where D is the damage varies from 0~0.99, and the crack initiation occurs as D is 0.99. ε_e is the equivalent creep strain rate, and ε_f^* is the multi-axial creep failure strain described by Cocks and Ashby [27]:

$$\frac{\varepsilon_f^*}{\varepsilon_f} = \frac{\sinh\{(2/3)[(n-0.5)/(n+0.5)]\}}{\sinh\{2[(n-0.5)/(n+0.5)]\sigma_m/\sigma_e\}} \tag{3}$$

where σ_m is the hydrostatic stress (mean normal stress) and ε_f the uni-axial creep failure strain. The damage ratio D considers the effect of stress triaxiality (hydrostatic stress, σ_m, divided by equivalent stress σ_e.)

The equivalent creep strain of the whole lattice truss panel structure ε_{eq} is calculated by:

$$\varepsilon_{eq} = \frac{\Delta h}{h} \tag{4}$$

where Δh is the creep deformation along tension or compression direction of the panel structure, and h is the initial total thickness of the lattice truss panel structure.

Stress analysis

At high temperature, the creep damage is affected by several stresses. The first is the as-brazed residual stress. The lattice truss sandwich panel structure is fabricated by high temperature brazing in a vacuum furnace. Due to the mismatching of material properties between filler metal and base metal, larger as-brazed residual stresses are generated [28, 29] and have a great effect on creep. During the brazing, the filler metal is pre-located between the face sheet and lattice core. A clamping fixture is designed to clamp the structure tightly and generates an applied load to ensure a close contact between face sheet and the lattice core. The structure is heated to 500 °C at 10 °C/min and holds for about 60 min. Then it is heated to the brazing temperature 1050 °C and holds about for 25 min. Finally, the assembly is cooled to the ambient temperature in the furnace. At the brazing temperature (1050 °C), the structure is at stress-free state. Therefore, the as-brazed residual stress is calculated during the cooling from 1050 °C to 20 °C. The total strain rate contains elastic, plastic and thermal strains. Elastic strain is calculated by the isotropic Hooke's law with temperature-dependent Young's modulus and Poisson's ratio. Thermal strain is calculated using the temperature-dependent CTE (coefficient of thermal expansion). The plastic strain is modeled by a rate-independent plastic model with Von Mises yield surface, temperature-dependent mechanical properties and isotropic hardening model (Table 1).

Table 1: Mechanical properties of 304 and BNi-2 [30, 31].

Material	Temperature (°C)	CTE ($1/°C \times 10^{-6}$)	Young's modulus (GPa)	Poisson's ratio	Yield strength (MPa)
304	20	16.0	199	0.28	206
	200	17.2	180	0.28	153
	400	18.2	166	0.28	108
	600	18.6	150	0.28	150
	800	19.5	125	0.28	125
BNi-2	20	13.4	205	0.28	300
	200	15.0	195	0.28	260
	400	16.8	184	0.28	220
	600	18.2	172	0.28	180
	800	19.9	161	0.28	160

The second stress is the operating thermal stress. The lattice truss sandwich structure is operated at 600 °C. Due to the different CTE, thermal stresses are calculated during the heating from 20 °C to 600 °C.

The third stress is induced by the operating mechanical load. A mechanical load was applied on the top surface of the face sheet, and the total stresses are calculated. This paper discusses the effects of tensile and compressive loads on the creep behavior. The final step is to calculate the creep damage for a service time of 50,000 h by considering the three types of stresses. In order to study the equivalent creep strain of the whole panel structure, a rigid solid plate was added on the top face sheet, in order to make the top face sheet have a uniform deformation along tensile or compressive direction because the core is porous. The load was applied on the rigid plate.

Material properties

The materials of face sheet and truss are 304 stainless steel, and the filler metal is BNi2. For the residual stress analysis, temperature-dependent mechanical properties of materials are incorporated. The material properties relevant to residual stress are elastic modulus, yield stress, Poisson's ratio and coefficient of thermal expansion, which are obtained from Refs [30, 31]. The creep parameters are listed in Table 2 [32].

Table 2: Creep parameters for 304 and BNi-2 at 600 °C [32].

Material	B	n
304	1.56×10^{-25}	9.03
BNi-2	8.75×10^{-40}	14.75

Boundary conditions

During the brazing, the structure is fixed tightly by the clamping in order to prevent mismatching and defects. During the creep analysis, the uniaxial creep test is modeled. Therefore, the symmetric boundary conditions were applied on the left and front face of the model, and the bottom face was constrained in Y-direction.

Results and discussion

Creep and damage distribution

Figure 4 shows the damage contour at tensile load at 50,000 h. The maximum damage is 0.99, which is located at the fillet. Therefore, the fillet becomes the potential failure position. Figure 5 shows the contours of equivalent creep strain (CEEQ) and stress triaxiality. The maximum CEEQ and stress triaxiality are 4.84 % and 1.17, respectively, which all locate at the fillet. Figure 6 shows the contour of initial total Mises stress before creep. The fillet has the maximum initial stress 193 MPa, which generates the maximum CEEQ. According to eq. (2), the damage is determined by CEEQ and stress triaxiality. Therefore, the maximum damage is generated at the fillet. Although the intersection points of the two trusses also have a larger stress triaxiality, while the CEEQ is very small. Therefore, the damage in the intersection of the two trusses is also very small. After 50,000 h, the equivalent creep strain of the whole lattice truss sandwich panel structure ε_{eq} is 2.84 %.

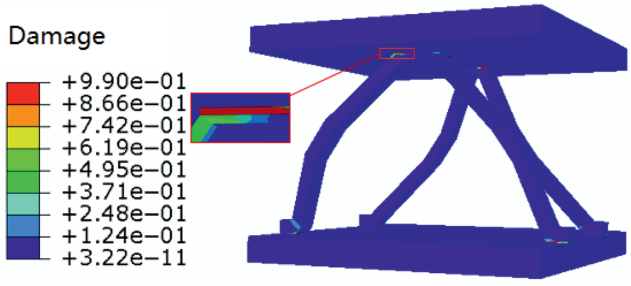

Figure 4: Damage contour at tensile load at 50,000 h.

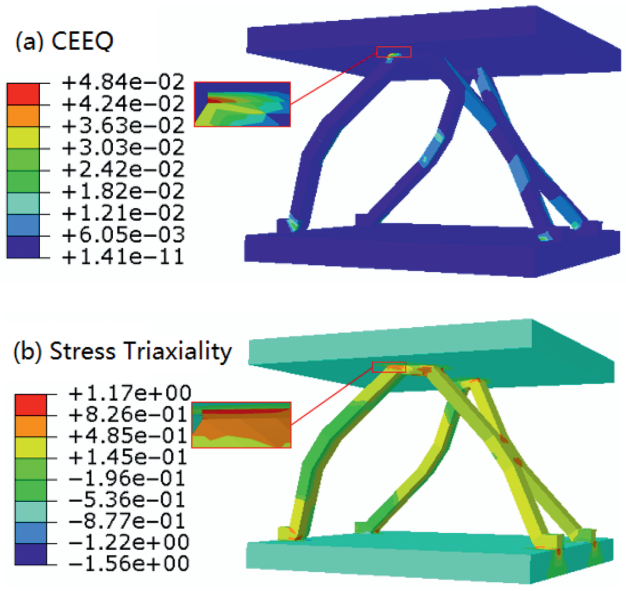

Figure 5: Contours of CEEQ (a) and stress triaxiality (b) at tensile load.

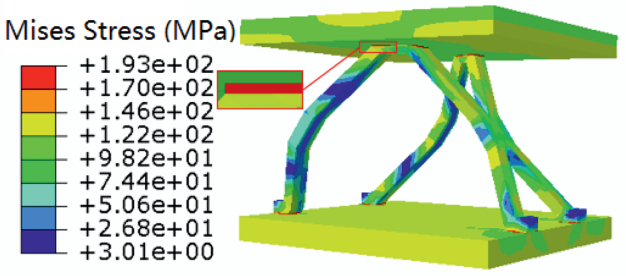

Figure 6: Contour of the initial total Mises stress.

Figure 7 shows the damage contour at compression load at 50,000 h. The maximum damage has reached the failure value 0.99 and also locates the fillet. Figure 8 shows the contours of CEEQ and stress triaxiality. The maximum CEEQ is 4.4 %, which decreases about 10 % compared to that at tensile load (Figure 5). The maximum stress triaxiality is 0.836, but it is located at the end of truss instead of

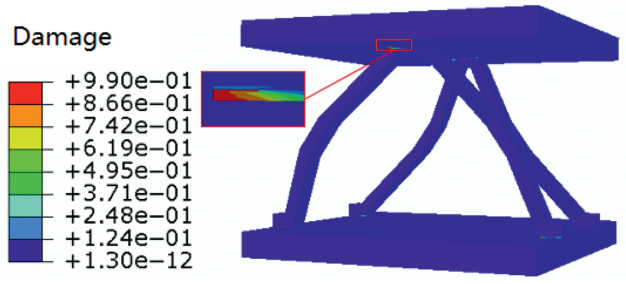

Figure 7: Damage contour at compression load at 50,000 h.

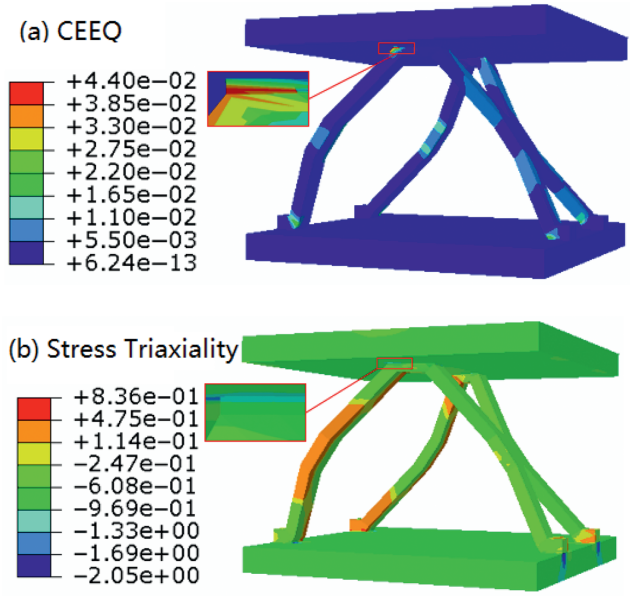

Figure 8: Contours of CEEQ (a) and stress triaxiality (b) at compression load.

the fillet. At compression load, the stress in the fillet is smaller than that at tensile load. Therefore, the creep at compression load is smaller than tension load.

Discussion

Based on the above results, it finds that the creep failure locates at the fillet at compressive and tensile loads. But due to the different stress distribution, the creep and stress triaxiality development are different. Figure 9 shows the maximum CEEQ and the stress triaxiality change with time for the same node at the fillet at compressive and tensile loads. It shows that the CEEQ and stress triaxiality at the tensile load are larger than those at compressive load, which proves that the brazing joint has a better creep resistance at compressive load. Therefore, the damage in the fillet at compressive state is far smaller than that at tensile state, as shown in Figure 10. At tensile load, the damage reaches the failure value 0.99 within 557 h. But at compressive load, it takes 27,300 h to reach the failure value 0.99. The damage rate at the fillet at tensile load is 50 times as much as that at compressive load. See Figure 9(a), the stress triaxiality almost keeps stable with time changing, while the CEEQ increases with the time changing (see Figure 9(b)), proving that the growth of creep strain is the dominant for damage. At compressive load, the stress triaxiality is negative value (~-0.8), therefore the damage grows very slowly. At tensile load, the stress triaxiality is a positive and accelerates the damage.

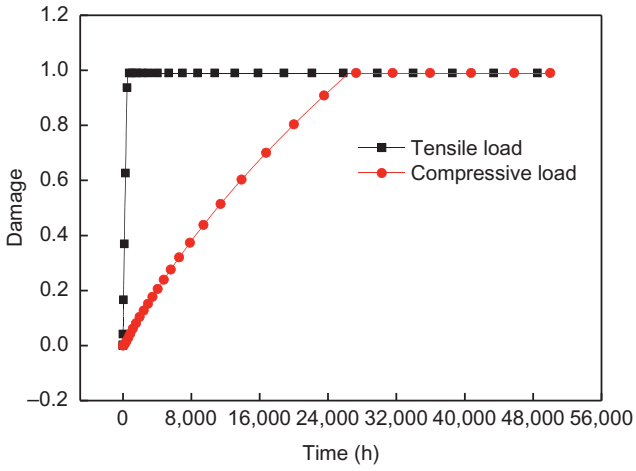

Figure 10: Damage change with time at the fillet at compressive and tensile loads.

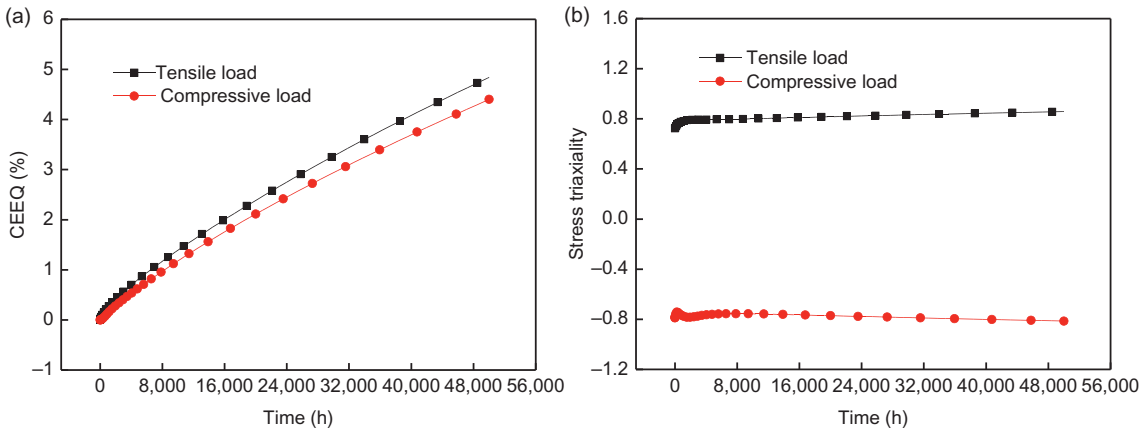

Figure 9: The maximum CEEQ (a) and stress triaxiality (b) change with time at the fillet for tensile and compressive loads.

Figure 11 shows the effect of the applied load on the damage at the fillet. It shows that the damage increases with the applied load increasing. In total, the damage value at compressive load is smaller than that at tensile state. At tensile state, as the load increases to 0.3 MPa, the damage value has reached the failure value 0.99, while it is still very small at compressive state. At the compressive load, the damage reaches the failure 0.99 until the load is 0.57 MPa. Figure 12 shows the effect of applied load on CEEQ at the fillet. It shows that the local maximum CEEQ increases with the applied load increasing. The CEEQ changes little as the applied load varies from 0.1 MPa to 0.4 MPa, but then it increases suddenly as the applied load increases from 0.4 MPa to 0.57 MPa.

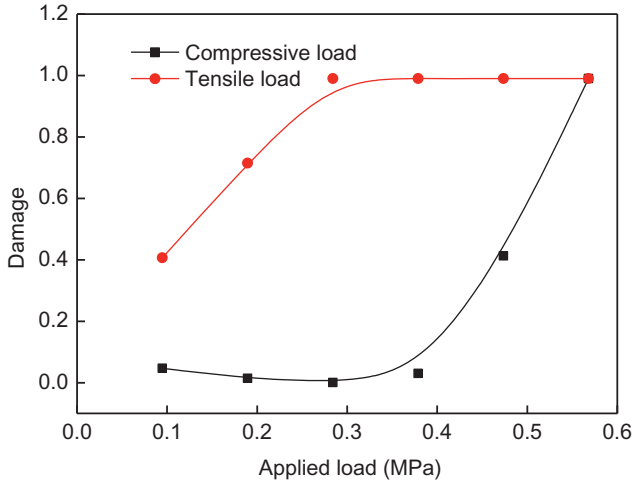

Figure 11: Effect of the applied load on the damage at compressive and tensile loads.

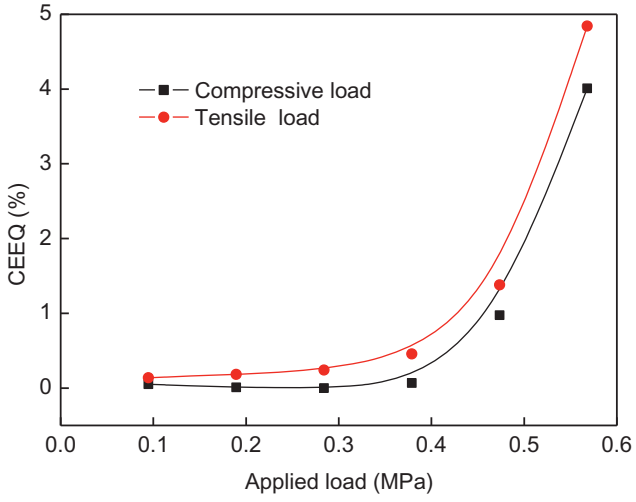

Figure 12: Effect of the applied load on the local maximum CEEQ at compressive and tensile loads.

At 0.57 MPa, the maximum local CEEQ is near 5 %. It also shows that the local maximum CEEQ at tensile load are larger than those at compressive load. Figure 13 shows the load effect on the equivalent creep strain of the whole panel structure. It shows that the equivalent creep strain increases slightly as the load increases from 0.1 to 0.4 MPa, but it has a sudden increase from 0.5 to 0.6 MPa. As the load is 0.57 MPa, the creep strain has been 2.84 %. Based on results of Figures 11–13, it concludes that for this model the limit load at tensile load and compressive load is 0.3 and 0.57 MPa, respectively.

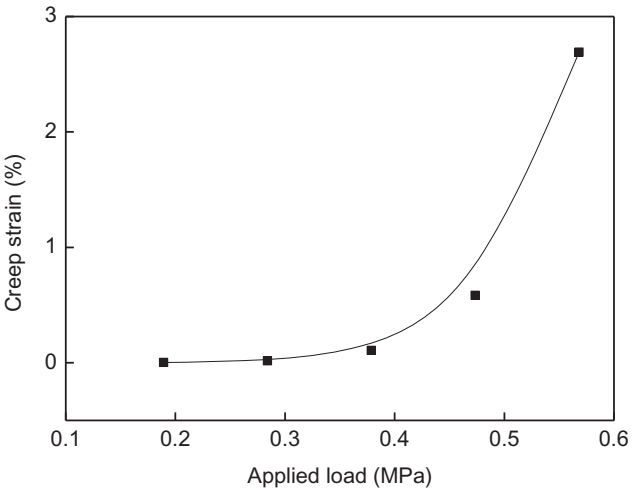

Figure 13: Effect of the applied load on the equivalent creep strain for the whole panel structure.

Lattice truss sandwich structure is also a type of cellular material. In recent years, great attention has been paid on its creep strength. Two analytical models have been developed to describe the creep behavior of the cellular material.

One is developed by Gibson and Ashby (GA model) [33]:

$$\dot{\varepsilon} = A\frac{0.6}{n+2}\left(\frac{1.7(2n+1)}{n}\right)\sigma^n\rho^{-(3n+1)/2}\exp\left(-\frac{Q}{RT}\right) \tag{5}$$

where σ is the uniaxial stress applied to the cellular material, ρ is the relative density. And the other parameters are related to the power law creep equation for the solid material of which the cellular material consists:

$$\dot{\varepsilon}_b = A\sigma_b^n\exp\left(-\frac{Q}{RT}\right) \tag{6}$$

where $\dot{\varepsilon}_b$ is the uniaxial strain rate, A is the creep constant, σ_b is the uniaxial stress, n is the stress component, Q is the creep activation energy, R is the gas constant and T is the temperature.

The other model is developed by Hodge and Dunand (HD model) [34]:

$$\dot{\varepsilon} = A\left(\frac{\rho}{3}\right)^{-n} \dot{\sigma}^n \exp\left(-\frac{Q}{RT}\right) \tag{7}$$

Here we compare the creep strain rate between the two models and our FEM result, as shown in Figure 14. It shows that the GA model is relatively closed to the present FEM result, while it has a big discrepancy compared to HD model. Because the truss bears the bending load mainly during the tensile or compressive loads, which is more suitable for GA model while HD model is used for the struts bear the compressive stress. But still there is a discrepancy between GA model and the present FEM. Because GA model is developed for the foam material, and the creep constitute equation is related to the relative density and independent on the dimension of truss, which leads to a large error.

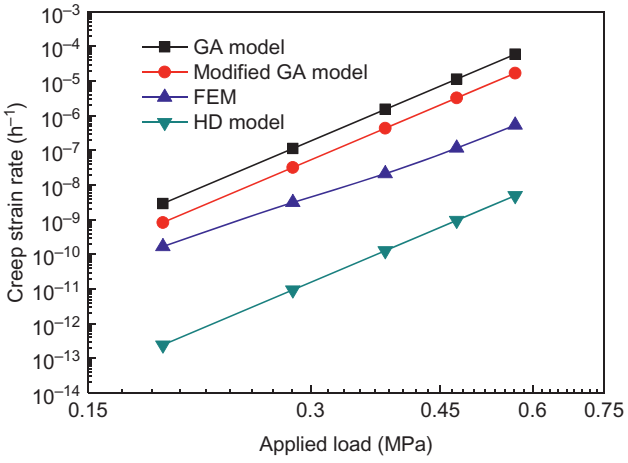

Figure 14: Load dependent creep rate by GA, HD, modified GA models and FEM.

In fact, the size effect on mechanical properties for the lattice truss sandwich structure is very notable. For this, Boonyongmaneerat and Dunand [35] developed a modified GA model (eq. 8) which considers the effect of strut dimension by a single parameter, the strut aspect ratio $a = 2d/k$ ($2d$ and k are strut length and width).

$$\dot{\varepsilon} = \frac{3.1}{n+2}\left(\frac{\dot{9.3}\cdot(2n+1)}{n}\right)^n \cdot \left[\left(\frac{a-1}{2}\right)^{2+n}\left(\frac{a+1}{2}\right)^{2n-1}\right] \cdot K\varepsilon^n \tag{8}$$

Figure 14 shows a comparison between our FEM result and the modified GA model. It shows that the modified model is much closed to FEM than GA model. But still there is a discrepancy because the modified GA model only considers the effect of the strut length and width. The other parameters such as truss thickness, the inclination angle and the thickness of face sheet have been ignored. In addition, in the above three models, the node dimension b shown in Figure 2 has also been ignored, and the node is assumed as rigid and the four trusses deform by creep bending, which also brings some error. As proved by Jiang et al. [28, 29], the size effect, including truss dimension, face sheet thickness and inclination angle, has a great effect on mechanical strength. We found that the as-brazed residual stresses increase as the face sheet thickness increasing. With truss thickness and truss length increase, the residual stresses decrease first and then increase. Therefore in the future, the size effect on creep should be investigated fully, and the GA model still needs to be improved to show the effect of all dimensions. In fact, it is very difficult to get an analytical model considering all the parameters. Therefore, a sensitivity study of parameters affecting creep deformation by finite element calculation to the unit cell should be performed in the future.

Conclusions

This paper studies the creep damage of an X-type lattice truss sandwich panel structure by finite element method and unit cell. The effects of as-brazed residual stress, operating thermal stress and mechanical load have been incorporated into the finite element model. Based on this study the following conclusions could be achieved.

(1) The creep failure is located at the fillet at tensile and compressive load. But at tensile load, the structure has a larger damage rate than that at tensile load. The damage rate of the fillet at tensile load is 50 times as much as that at compressive load.

(2) The lattice truss sandwich panel structure has a better creep resistance to compressive load than tensile load, because the stress triaxiality at the fillet has been decreased at compressive load. The creep strain and damage increase as the applied load increases.

(3) The equivalent creep rate calculated by finite element method and several analytical models have been compared. The results show that compared with Gibson–Ashby model and Hodge–Dunand models, the modified GA model has a good prediction result compared with finite element method. But still there is a discrepancy for the modified GA model, because it doesn't consider the dimension effect. A more accurate model considering the size effect still needs to be developed.

Acknowledgments: The authors gratefully acknowledge the support provided by Taishan Scholar Construction Funding (ts201511018) and Natural Science Foundation for Distinguished Young Scholars (JQ201417) of Shandong Province, National Natural Science Foundation of China (11372359) and Fundamental Research Funds for the Central Universities (14CX05036A and 15CX08006A).

References

[1] J.-S. Huang and L.J. Gibson, Mat. Sci. Eng. A., 339 (2003) 220–226.
[2] D.T. Queheillalt and H.N.G. Wadley, Mater Des., 30 (2009) 1966–1975.
[3] H.L. Fan, F.N. Jin and D.N. Fang, Mater. Des., 30 (2009) 511–517.
[4] T.J. Lu, L. Valdevit and A.G. Evans, Prog. Mater. Sci., 50 (2005) 789–815.
[5] T. Wen, J. Tian, T.J. Lu, D.T. Queheillalt and H.N.G. Wadley, Int. J. Heat. Mass. Trans., 49 (2006) 3313–3324.
[6] P. Beiss, E. El-Magd and J. Stuhrmann, Comp. Mater. Sci., 47 (2009) 213–219.
[7] Y. Mizokami, T. Igari, F. Kawashima, N. Sakakibara, M. Tanihira, T. Yuhara and T. Hiroe, Nucl. Eng. Des., 255 (2013) 248–262.
[8] W. Jiang, J. Gong, S. Tu and Hu. Chen, J. Mater. Process Tech., 209 (2009) 1105–1110.
[9] L.E. Herranz, J.I. Linares and B.Y. Moratilla, Appl Therm Eng, 29 (2009) 1759–1765.
[10] G. Chen, G.Z. Wang, J.W. Zhang, F.Z. Xuan and S.T. Tu, Eng. Failure Anal., 47 (2015) 56–66.
[11] L.A. Spyrou, P.I. Sarafoglou, N. Aravas and G.N. Haidemenopoulos, Eng. Failure Anal., 45 (2014) 456–469.
[12] N. Ohno, K. Narita and D. Okumura, Int. J. Heat Mech. Sci., 86 (2014) 18–25.
[13] M. Tsuda and N. Ohno, Int. J. Plasticity, 27 (2011) 1560–1576.
[14] M. Tsuda, E. Takemura, T. Asada, N. Ohno and T. Igari, Int. J. Mech. Sci., 52 (2010) 648–656.
[15] N. Ohno, K. Ikenoya, D. Okumura and T. Matsuda, Int. J. Solids. Struct., 49 (2012) 2799–2806.
[16] F. Kawashima, T. Igari, Y. Miyoshi, Y. Kamito and M. Tanihira, Nucl. Eng. Des., 237 (2007) 591–599.
[17] G.-Y. Zhou and S.-T. Tu, Int. J. Solids Struct., 44 (2007) 6791–6804.
[18] W. Jiang, J. Gong, Hu. Chen and S.T. Tu, Int. J. Pres. Ves. Pip., 85 (2008) 569–574.
[19] W.C. Jiang, J.M. Gong, S.D. Tu and H. Chen, Mat. Sci. Eng. A., 499 (2009) 293–298.
[20] S.M. Oppenheimer and D.C. Dunand, Acta Mater., 55 (2007) 3825–3834.
[21] E. El-Magd, J. Gebhard and J. Stuhrmann, Comp. Mater. Sci., 39 (2007) 446–452.
[22] Q. Zhang and T. Lu, Acta. Mech. Solida. Sin., 25 (2012) 111–116.
[23] G.W. Kooistra and H.N.G. Wadley, Mater. Des., 28 (2007) 507–514.
[24] J.-F. Wen and S.-T. Tu, Eng. Fract. Mech., 123 (2014) 197–210.
[25] G. Chen, G.Z. Wang, F.Z. Xuan and S.T. Tu, Mater. Des., 63 (2014) 600–608.
[26] L. Zhao, H. Jing, L. Xu, Y. Han and J. Xiu, Eng. Fract. Mech., 110 (2013) 233–248.
[27] A.C.F. Cocks and M.F. Ashby, Metal. Sci., 14 (1980) 395–402.
[28] W. Jiang, H. Chen, J.M. Gong and S.T. Tu, Mat. Sci. Eng. A., 528 (2011) 4715–4722.
[29] B. Wen-chun Jiang, B.Y. Yang, W.H. Chen and J.M. Gong, Mater. Des., 49 (2013) 1048–1055.
[30] W. Jiang, Z. Liu, J.M. Gong and S.T. Tu, Int. J. Pres. Ves. Pip., 87 (2010) 457–463.
[31] K.S. Weil and B.J. Koeppel, J. Power. Sources., 180 (2008) 343–353.
[32] J. Shi, S-D Tu and J. Gong, Mater. Mech. Eng., 7 (2005) 20–24.
[33] E.W. Andrews, L.J. Gibson and M.F. Ashby, Acta Mater., 47 (1999) 2853–2863.
[34] A.M. Hodge and D.C. Dunand, Mater. Trans. A, 34 (2003) 2353–2363.
[35] Y. Boonyongmaneerat and D.C. Dunand, Acta Mater., 57 (2009) 1373–1384.